

BEARING CAPACITY AND FAILURE MECHANISM OF NONWOVEN GEOTEXTILE REINFORCED CLAY: A VERIFICATION

Minh-Duc Nguyen^{a,*}

^a*Faculty of Civil Engineering, Ho Chi Minh City University of Technology and Education,
1 Vo Van Ngan street, Linh Chieu ward, Thu Duc City, Ho Chi Minh City, Vietnam*

Article history:

Received 17/02/2022, Revised 16/6/2022, Accepted 20/6/2022

Abstract

The paper presents a series of laboratory tests for California Bearing Ratio (CBR) to investigate the bearing capacity and the failure mechanism of nonwoven geotextile reinforced clay. The variation of the tests included the number of reinforcement layers and compaction energy. The results indicate that the nonwoven geotextile layers improve up to 49.5% of the CBR of the reinforced clay specimens. A cross-grab stick apparatus was developed to determine the deformed shape of the embedded reinforcement layer in the reinforced specimens after CBR tests. The obtained results illustrate the membrane tension effect of the geotextile layers to enhance the bearing capacity of the reinforced soil specimens. Last, the failure mechanisms of the nonwoven geotextile reinforced specimens were verified using measurement results of maximum relative deflection in reinforcement layers.

Keywords: nonwoven geotextile; California bearing ratio; bearing capacity; reinforced clay; failure mechanism.

[https://doi.org/10.31814/stce.huce\(nuce\)2022-16\(3\)-10](https://doi.org/10.31814/stce.huce(nuce)2022-16(3)-10) © 2022 Hanoi University of Civil Engineering (HUCE)

1. Introduction

The increasing demand for transportation development has led to more roads being constructed in the rural areas of the Mekong Delta region, Vietnam. For these projects, a cost-effective method is to use clay excavated from the Mekong River as backfill soil. In addition to representing a green and sustainable development solution, other advantages include (1) the avoidance of the environmental effects of the clay extracted through the dredging process, (2) the reduction in using natural sand, and (3) decrease in the cost of construction. However, the stability of the reinforced clay structure was questionable, requiring a study of the bearing capacity and failure mechanisms of these structural types.

To investigate the bearing capacity of reinforced clay, numerous studies have employed laboratory and in-situ tests for the California bearing ratio (CBR) because of its applicability to a wide range of different materials and remold specimens. The CBR value is a common index property used to evaluate the strength and resilient modulus of subgrade soil and base course materials for designing the pavement structure [1]. For reinforced soil, the CBR test was applied to investigate the effects of geogrids [2–7] and geotextiles [8–10] on improving its bearing capacity.

*Corresponding author. *E-mail address:* ducnm@hcmute.edu.vn (Nguyen, M.-D.)

In particular, the influence of reinforcement spacing on enhancing the bearing capacity of reinforced clay was presented in the previous studies. When using geosynthetic clay liners (GCLs) reinforced with a single reinforcement layer, the highest CBR improvement was observed in the GCL specimens with a sand layer thickness equal to that of the diameter of the loaded piston [8]. In contrast, using a single layer of either geogrid or jute fabric, other studies illustrated that placing a single reinforcement layer in the middle of the base layer was the most effective for reducing the settlement of reinforced pavement [2, 4, 6]. In another study, the geosynthetic reinforcement layer should be placed either at mid-specimen height or between the upper one-third and middle layers to achieve the highest CBR value [7]. For clean sand, sandy clay, and clayey silt, the optimal location of a single geogrid layer was at 72% to 76% of the specimen height of reinforced soil specimens [3].

In addition, the CBR values of clay reinforced using varying numbers of reinforcement layers have been investigated in other studies. Two-layer geogrid reinforcement only marginally improved the strength over single-layer reinforcement when placed close to mid-depth from the top of the compacted soil specimens [5]. However, when performing the CBR tests by using a nonwoven geotextile with high-tenacity polyester yarns and reinforced fine soil under soaking conditions, the laboratory measurement demonstrated that the bearing capacity of the geosynthetic reinforced specimens was higher than that of the unreinforced samples; the increment in the number of reinforcement layers induces the higher the bearing capacity of the geosynthetic reinforced specimens. This bearing capacity improvement was attributed to tension mobilized in the reinforcement layers membrane. And the alternate surface failure enhancing the shear strength was attributed to the effect of the reinforcement layers [9]. It believes that differences in failure mechanisms induced the various optimum reinforcement arrangement.

Investigations into the failure mechanism of geosynthetic reinforced soil have also been conducted previously, which depends on the distance from the bottom of a foundation to the first reinforcement layer, d_1 , the width of foundations, and the reinforcement spacing, h . Table 1 summarizes the failure mechanisms of the reinforced soil proposed by various studies. In failure mode 1, the soil would fail along the failure surface above the top reinforcement layer [11]. In that case, the failure would occur when the thickness of the top layer of soil was greater than half of the foundation width (B). In the case of reinforcement spacing h greater than $0.5B$, the reinforced soil could also fail as a result of soil slippage between the reinforcement layers [12]. If both the topsoil layer and reinforcement spacing are less than $0.5B$, the reinforced soil would first undergo a punching shear failure followed by a general shear failure [13, 14]. Based on these three potential failure modes, several analytical solutions

Table 1. Failure mode of geosynthetic reinforced soil [11–14]

Failure mode	Distance from foundation to the first reinforcement layer, d_1	Reinforcement spacing, h	Foundation failure description
Mode 1	$d_1 > 0.5B$	any value	Failure above top reinforcement layer
Mode 2	$d_1 < 0.5B$	$h > 0.5B$	Failure between reinforcement layers
Mode 3	$d_1 < 0.5B$	$h < 0.5B$	Punching shear failure followed by general shear failure

have been developed to predict the bearing capacity of reinforced soil [14, 15]. However, studies verifying the failure modes of reinforced soil through the analysis of soil movement and reinforcement deformation remain limited.

In this study, a series of laboratory tests were performed to examine the CBR behavior of clay reinforced with a nonwoven geotextile. The unreinforced and reinforced specimens were compacted at the optimum moisture content of the clay of which the degree of saturation, S_r was less than 86% (Table 2). After CBR tests, the upper soil layers in the nonwoven reinforced specimens were dismantled to uncover the embedded reinforcement layers. Using a cross-grab stick apparatus, the vertical deflections of those reinforcement layers were measured in longitudinal and transfer directions to determine their deformed shapes after CBR tests. The obtained results would reveal the bearing capacity behavior and failure mechanisms of nonwoven geotextile reinforced clayey soil, which would clarify the optimum reinforcement arrangement to gain the highest bearing capacity of the reinforced clay.

2. Experimental Program

A total of 30 laboratory CBR tests were performed to determine the bearing capacity of nonwoven geotextile reinforced clay. Variations in the test included the number of reinforcement layers and compaction energy levels.

2.1. Test materials

a. Riverbed clay

The dredging clay was excavated from Cai Lon River, Kien Giang Province, Vietnam. The clay is classified as high plastic inorganic silt using the Unified Soil Classification System (USCS). The properties of the clay are listed in Table 2.

Table 2. Soil properties

Property	Value			
Soil name (USCS)	MH			
Plastic limit, PL (%)	44.9			
Plastic index, PI (%)	46.6			
Liquid limit, LL (%)	91.5			
Specific gravity, G_s	2.75			
Free swell index (%)	55.9			
Modified Proctor compaction test				
Compaction energy, E (kJ/m ³)	Total number of blows	ω_{opt} (%)	γ_{d-max} (kN/m ³)	Degree of saturation, S_r (%)
482	50	26.6	14.28	82.3
1200	125	24.5	15.11	85.8
2700	280	20.5	16.15	84.1

Following ASTM D1557 [16], the modified Proctor test was performed to determine the optimum moisture content, ω_{opt} , and maximum dry unit weight of the clay, γ_{d-max} , which would be used later for preparing specimens in the CBR test. With a mold 15.24 cm in diameter, 116.6 mm in height,

and a modified Proctor rammer (44.48 N drop from 457.2 mm), the soil specimens were compacted using the three compaction energy levels (E) 2700, 1200, and 482 kJ/m^3 . The compaction curves were presented in Fig. 1, of which the value of $\gamma_{d-\max}$ and ω_{opt} were given in Table 2. It shows that the increment of E induces the raise of $\gamma_{d-\max}$ and the reduction in ω_{opt} .

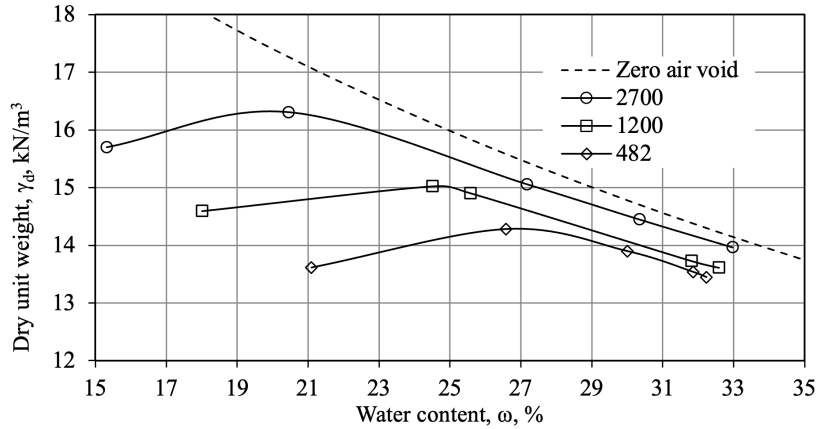


Figure 1. The compaction curves under 2700 kJ/m^3 ; 1200 kJ/m^3 and 482 kJ/m^3 of compaction energy levels

b. Geotextile

A commercially available needle-punched polyethylene terephthalate nonwoven geotextile was used, the properties of which are presented in Table 3. This geotextile had a permittivity equal to 1.96 s^{-1} , and a corresponding cross-plane permeability equal to 3.5×10^{-3} m/s which is higher than the permeability of the compacted clay. The load-elongation behavior of reinforcement was determined using the wide-width tensile test in the longitudinal and transverse directions [17]. The experimental results revealed the anisotropic tensile behavior of the geotextile.

Table 3. The properties of nonwoven geotextile [17]

Property	Value		
Fabrication process	Needle-punched PET nonwoven geotextile		
Mass (g/m^2)	200		
Thickness (mm)	1.78		
Apparent opening size (mm)	0.11		
Permittivity (s^{-1})	1.96		
Cross-plane permeability (m/s)	3.5×10^{-3}		
Wide-width tensile test			
Direction	Strength at break (kN/m)	Elongation at break (%)	Secant stiffness at peak strength (kN/m)
Longitudinal	9.28	84.1	11.03
Transverse	7.08	117.8	6.01

2.2. Specimen preparation

The soft clayey soil was excavated from the riverbed and dried in an oven at a temperature of less than 60 °C for more than 24 h to prepare dried soil as suggested in ASTM 1883 [18]. Using a mortar, the dried soil was then crushed and ground into powder. Based on the optimum moisture listed in Table 2, the moisture soil specimens were made by mixing clay powder with water. After mixing, the soil was stored in a resealable plastic bag in a temperature-controlled chamber for a minimum of 2 days, to allow the moisture to be distributed uniformly within the soil mass.

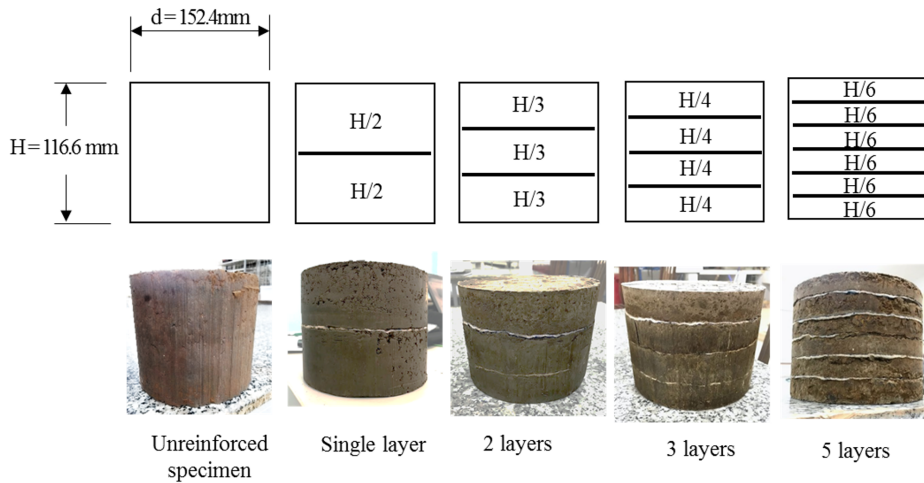


Figure 2. Geotextile arrangement in specimens

Both unreinforced and nonwoven geotextile reinforced specimens were prepared in a mold with a diameter, $D = 152.4$ mm, and a height, $H = 116.6$ mm. For the unreinforced specimens, the number of blows and the amount of soil per compaction layer were evaluated using the results of the modified Proctor compaction test. The last compacted layer should be slightly above the mold's top but not more than approximately 6 mm [16]. A knife was used to trim compacted specimens for evenness with the top of the mold. The top surface was flatted by filling any holes with uncompacted soil.

As shown in Fig. 2, the reinforced specimens were prepared by compacting and stabilizing with one, two, three, and five reinforcement layers (Fig. 2). After compacting and leveling the soil layers, they were scarified before placing a 152.4-mm-diameter dry geotextile layer horizontally on the roughened surface. The next soil layer was then poured and compacted. Last, the surface of the reinforced specimens was constructed using the same process as that of the unreinforced specimens.

In the field, the soft clay should be dried to reduce the water content and compacted at its optimum moisture content. The reinforced soil structures including mechanically stabilized earth (MSE) walls and reinforced soil slopes (RSS) were then constructed by placing alternating layers of reinforcement and compacted soil behind a facing element to form a composite material that acts integrally to restrain lateral forces [19]. A similar construction method was also applied when using the geosynthetics reinforced soil for the flexible pavements. The attraction of this application lies in the possibility of reducing the thickness of the base course layer such that a roadway of equal service life results or in extending the service life of the roadway [20].

2.3. Testing program

The laboratory test for the CBR value was performed following ASTM D1558 [18]. The same surcharge mass (4.54 kg) was placed on the specimens before applying the load on the penetration piston with a diameter, $B = 49.7$ mm. The ratio between the diameter of reinforcement and penetration piston D/B in this study was approximately 3.1, which is slightly less than the optimal value, $D/B = 3.15\text{--}3.80$ for obtaining the highest bearing capacity for a circular reinforced foundation [21]. In addition, the ratio of the reinforcement spacing and the penetration piston, h/B is varied between 0.4 to 1.2, which would be able to cover all failure modes presented in the previous section.

The penetration rate of the piston was approximately 0.05 in/min (1.27 mm/min), and the tests were halted when at a penetration diameter of 20 mm. In most cases, the zero point of the stress-penetration curves were adjusted owing to surface irregularities or other causes, as recommended in [18]. Consequently, the corrected penetration of the tests would be less than the actual penetration of the piston at the end of the tests.

The CBR value can be obtained as follows:

$$CBR_1(\%) = \frac{P_1}{6900} \times 100 \quad (1)$$

$$CBR_2(\%) = \frac{P_2}{10300} \times 100 \quad (2)$$

in which P_1 and P_2 are the stresses in kPa on a piston at 2.54 and 5.08 mm after corrected penetration, respectively. Based on ASTM 1883, the CBR value is chosen as the higher value of CBR_1 and CBR_2 [18].

2.4. Measurement of the vertical deflection and deformed shape of nonwoven geotextile layers in the reinforced specimens

The piston penetration in the CBR test causes concave deformation of the nonwoven geotextile layers embedded in the reinforced specimens (Fig. 3(a)). After the CBR test, the upper soil layers were peeled off to uncover the embedded nonwoven geotextile layers in the reinforced specimens. The deformed shape of the reinforcement layers was captured through measurement of the vertical deflection at different points along with the longitudinal and transverse directions of the layers using a cross-grab stick apparatus. The device consists of thirty-seven firm sticks 160 mm in length those were held vertically to the cross-section of the specimens. To facilitate this, holes were pierced on a cross-shaped plate, the dimension of which is depicted in Fig. 3(b) along with the distribution of the holes. The bottom of the firm sticks firmly contacted the surface of the reinforcement layers. The deformed shape of reinforcement layers was sketched through measurement of the relative deflection of the heads of the rigid bars. First, the specimens were placed on a horizontal surface. Through the employment of a fixed linear variable differential transformer (LVDT), the altitude of the head of each stick was measured, with the specimens moved to the position at which the head of the bar reached the head of the LVDT (Fig. 3(a)). The relative vertical deflection of a point on a reinforcement layer δ_i was determined using a comparison of its altitude with that of a point located at the periphery of the specimens. Thus, the absolute altitude of a point z'_i , defined as the vertical distance from the bottom of the specimen to that point on the deformed reinforcement layer i after the test, was evaluated as follows:

$$z'_i = z_i - \delta_i \quad (3)$$

where z_i is the absolute altitude of a point along the periphery of the reinforcement layer i in the reinforced specimens after the CBR test. Because the distance from the center to the periphery of the mold (i.e., the mold radius) was approximately $1.5B$, the stress at the periphery of the specimen was close to zero [22]. This finding supported the assumption that accounted for nonvertical settlement at points along the edge of the reinforcement layers after the CBR tests.

$$z_i = \left(1 - \frac{i}{n + 1}\right)H \quad (4)$$

where H is total height of the specimens and was 116.6 mm.

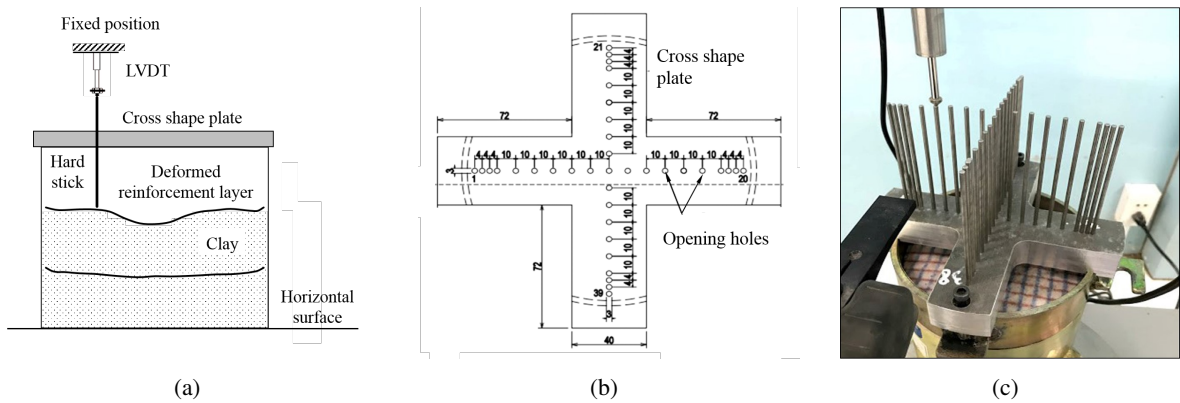


Figure 3. The vertical deflection measurement of the deformed nonwoven geotextile layers (a) schematic measurement; (b) cross shape plate (dimension in mm); (c) cross-grab stick apparatus in measurement process

3. Results and Discussion

3.1. CBR values of unreinforced and nowoven geotextile reinforced specimens

The CBR results of unreinforced and nowoven geotextile reinforced clay specimens are summarized in Table 4. The CBR values were significantly improved when reinforced clay specimens with nonwoven geotextile layers. A similar finding has been reported in numerous studies [3, 4, 6–9, 23, 24].

To quantify the bearing capacity improvement of the reinforced clay specimens, the percent CBR improvement due to reinforcement effects was calculated as follows:

$$\% \Delta CBR = \frac{CBR_{re} - CBR_{unre}}{CBR_{unre}} \times 100\% \quad (5)$$

where the CBR_{un} and $CBR_{reinforced}$ are the CBR value of the unreinforced and reinforced specimens, respectively.

As shown in Table 4, the percent CBR improvement of the reinforced specimens, $\% \Delta CBR$ was varied depending on the number of geotextile layers and the compaction energy. It reached the highest value, $\% \Delta CBR = 49.5\%$ when the clay specimen was compacted under compaction energy $E = 482 \text{ kJ/m}^3$ and reinforced by two nonwoven geotextile layers.

The improvement of the shear strength and the bearing capacity of the geosynthetic reinforced specimens was attributed to the soil-reinforcement interaction in the specimens [9]. The reinforcement

layers acted to restrain the lateral deformation resulting from the interfacial shear stress between the soil and reinforcement. In addition, the membrane tension developed an upward force inducing an increase in the bearing capacity, manifesting in the concave deformation in the reinforcement layers of the reinforced specimens after the tests [9, 15, 25].

The bearing capacity of the reinforced specimens depended heavily on the depth of the top reinforcement layer d_1 . As presented in Table 4, for all of the compaction energy, the CBR values of the reinforced specimens were the highest when the specimens were reinforced with two nonwoven geotextile layers, of which the reinforcement spacing value was equal to the depth of the top reinforcement layer, $h = d_1 = 38.8$ mm. In other words, the ratio $d_1/B = 0.78$ was the optimum ratio to obtain the highest CBR for the nonwoven geotextile reinforced clay specimens. It should be noted that the CBR values were evaluated using the pressure on the piston at small penetration (i.e., at 2.54 and 5.08 mm). At the higher penetration of the piston, the reinforcement layers at higher depths were mobilized to increase the bearing capacity of the reinforced specimens. At up to 15 mm of piston penetration, the increment of the number of reinforcement layers induced an increment in the bearing capacity of the reinforced soil (Table 4).

Different optimal values for d_1/B have been reported in other studies. For example, the soil thickness required to cover a geosynthetics reinforced clay liner must be at least equal to the diameter of the load piston (i.e., $d_1/B = 1$) [8]. A similar conclusion has been presented following the conduction of CBR tests on expansive soil subgrades reinforced with a single reinforcement layer [4, 6]. However, a geogrid layer placed at a depth of approximately 1 to 1.2 times the diameter of the plate load attained the highest CBR value among reinforced specimens [3]. In the case of a higher number of reinforcement layers, increasing the number of reinforcement layers from one to two led to the higher CBR behavior of the geosynthetic-reinforced fine soil [7, 9].

Table 4. CBR values, dry unit weights of unreinforced and reinforced specimens

Cases	Compaction energy (kJ/m ³)	Dry unit weight, kN/m ³	CBR value (%)	% CBR improvement	Correct stress at 15 mm of penetration (kPa)
Unreinforced	482	13.61	9.5	0.0	1241
1 layer	482	13.71	12.3	29.5	1729
2 layers	482	13.94	14.2	49.5	2122
3 layers	482	14.47	11.7	23.2	2224
5 layers	482	14.66	10.8	13.7	2357
Unreinforced	1200	15.11	17.3	0.0	2284
1 layer	1200	15.19	19.3	11.6	3100
2 layers	1200	15.25	24.7	42.8	3209
3 layers	1200	15.80	19.8	14.5	3360
5 layers	1200	16.06	18.6	7.5	3496
Unreinforced	2700	16.15	40.1	0.0	4935
1 layer	2700	16.23	44.2	10.2	7015
2 layers	2700	16.38	51.8	29.2	7121
3 layers	2700	16.71	45.9	14.5	7232
5 layers	2700	16.86	43.2	7.7	7358

3.2. Deformation shape of nonwoven geotextile layers

In the measurement results of the deformed shape of the nonwoven geotextile layers in the specimens, a marginal difference was noted between the absolute altitudes of the reinforcement discs along the two directions after the CBR tests. A similar observation was made for the deformed reinforcement layers of the reinforced specimens compacted under the other compaction energy levels. This finding verified that axisymmetric deformation occurred in the reinforcement layers of the reinforced specimens as a result of the piston penetration in the CBR test; this was consistent with the deformation in a nonwoven geotextile after a puncture strength test [26]. This test involved a 50-mm-diameter piston penetrated into a reinforcement layer clamped on a modified CBR mold with an inside diameter of 150 mm.

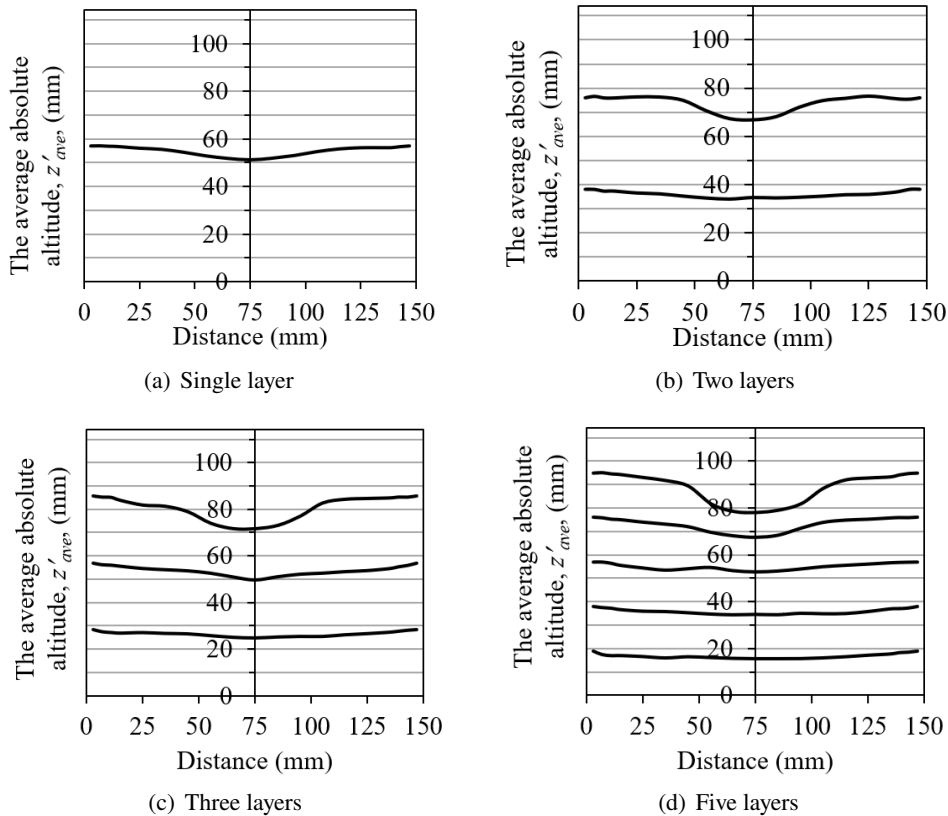


Figure 4. Average deformed shape of nonwoven geotextile layers in specimens compacted using compaction energy, $E = 486 \text{ kJ/m}^3$

Figs. 4 to 6 depict the average absolute altitude of the reinforcement layer z'_{ave} evaluated from the absolute altitudes measured along the longitudinal and transverse directions of the reinforcement layers after the CBR test. For the nonwoven geotextile reinforced specimens compacted using the three compaction energy, the reinforcement layers exhibited concave deformation, in which the maximum vertical deflection was located at the center of the reinforcement layers. That finding was consistent with those on the tensile strain distribution on geogrid layers in reinforced sand foundations [27] and stress distribution [22] in reinforced sand specimens, in which the maximum tensile strain and stresses were concentrated beneath the center of the footing in reinforced soil. Furthermore, the more vertical

deflection was observed in the reinforcement layers located at a shallower depth, which was closer to the piston. The deformed concave shape of reinforcement layers demonstrated the membrane tension creating an upward force and enhancing the bearing capacity of the reinforced specimens. Related studies have already reported and verified the membrane tension effect and its capacity to enhance reinforced soil foundation bearing capacity [11, 12, 28].

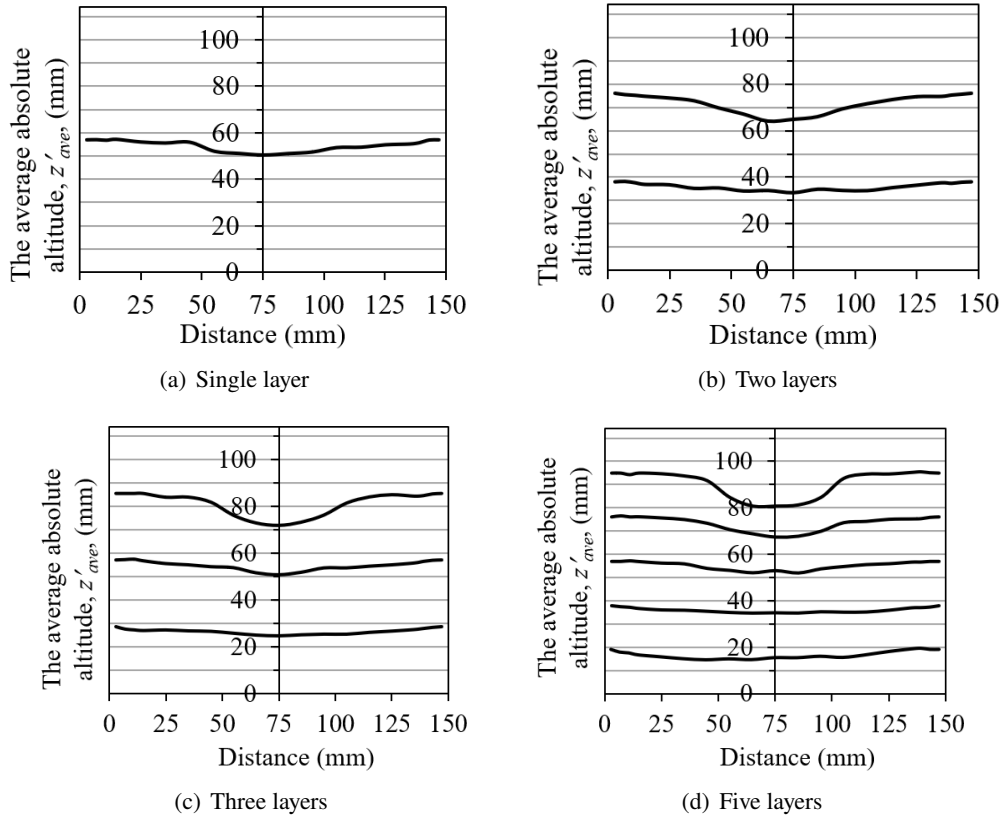


Figure 5. Average deformed shape of nonwoven geotextile layers in specimens compacted using compaction energy, $E = 1200 \text{ kJ/m}^3$

Fig. 7 presents the maximum deflection of the nonwoven geotextile layers in the specimens compacted using the three compaction energy levels. The maximum deflection ratio of the deformed reinforcement layers (i.e., the deflection ratio at the center of the reinforcement layers) R_δ was defined as the ratio of maximum vertical deflection of a reinforcement layer and piston penetration at the end of the CBR test. As shown in Fig. 7, the maximum deflection sharply decreased when the depth of the reinforcement layers increased. In particular, R_δ decreased from 0.82 to less than 0.4 when the depth of the reinforcement layers increased from $0.4B$ to $1.2B$. For the nonwoven geotextile reinforcement layers were deeper than $1.6B$, the maximum deflection of the reinforcement layers was low, in which the maximum deflection ratio was approximately 0.1 to 0.3. A similar tensile strain of the geogrid layer was observed in the shallow square footings of geogrid-reinforced sand; at the same foundation settlement, this was significantly reduced when the depth of the first layer increased from $0.3B$ to $0.9B$ [27]. On the other hand, the increment in compaction energy and clay density of the nonwoven geotextile reinforced specimens did not induce any significant difference in the maximum

deflection of the nonwoven geotextile layers (Fig. 7).

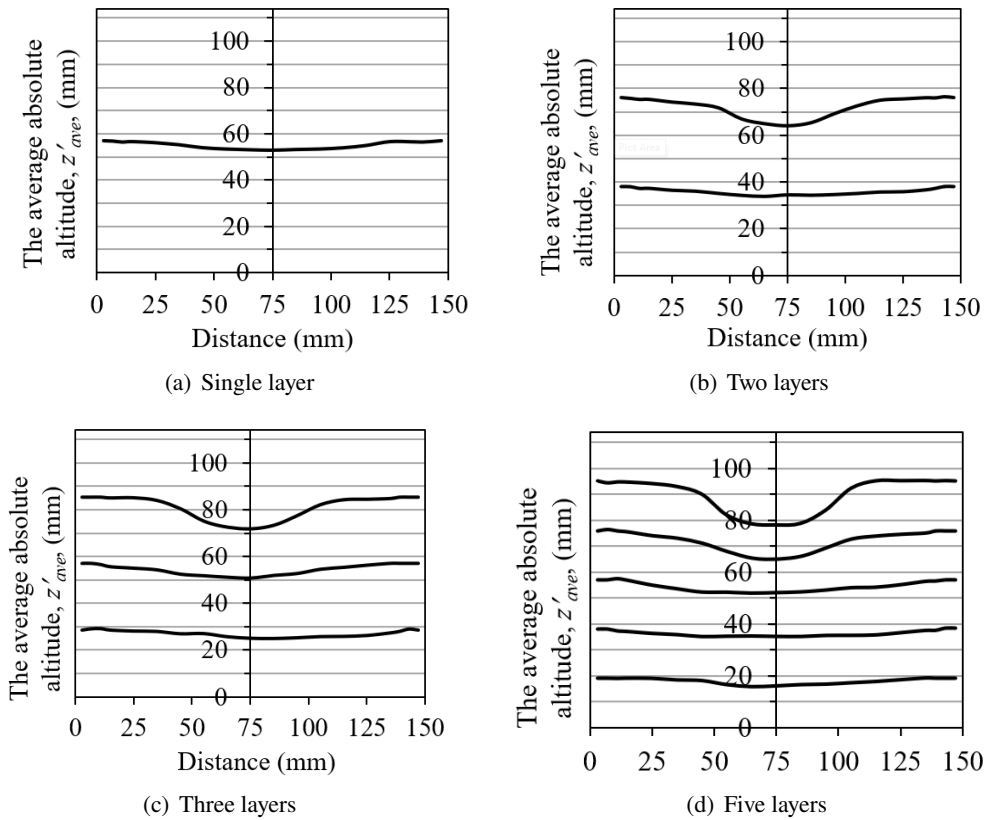


Figure 6. Average deformed shape of nonwoven geotextile layers in specimens compacted using compaction energy, $E = 2700 \text{ kJ/m}^3$

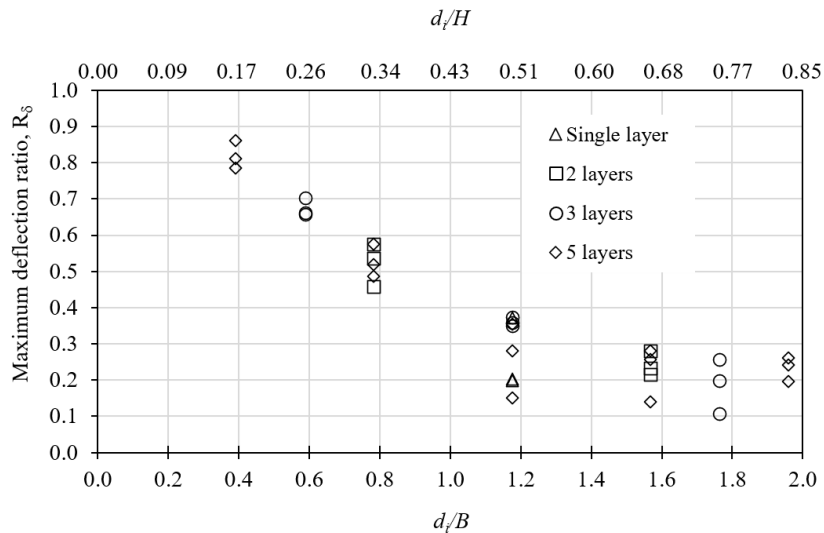


Figure 7. The maximum deflection ratio of nonwoven geotextile layers in specimens compacted using three compaction energy, 486, 1200, and 2700 kJ/m^3

3.3. Failure modes of reinforced soil specimens

The reinforcement deformation results in the reinforced specimens were used to verify the failure mechanism of the reinforced soil under the CBR test condition. Other studies have introduced three failure modes of the reinforced foundation, namely (i) failure above the top reinforcement layer, (ii) failure between the reinforcement layers, and (iii) punching shear failure followed by general shear failure. Failure Mode 1 was described as the failure surface that occurs above the top layer when the depth of the first layer d_1 is greater than $0.5B$ [11]. When the reinforcement spacing h is greater than $0.5B$, the failure occurs between the reinforcement layers [12]. For a d_1 and h less than $0.5B$, the punching shear failure initially occurs in the reinforced zone, and then the general shear failure surface occurs below the last reinforcement layer [15].

As discussed, the penetration of the piston induced concave deformation in the reinforcement layers. Consequently, the distance between the piston (i.e., the foundation) and top reinforcement layer d_1 also changed during the CBR test. Because the maximum vertical deflection of the reinforcement occurred at the center of the reinforcement layers, the maximum vertical distance between the piston and top reinforcement layer after 20-mm piston penetration d'_1 could be determined using the maximum relative deflection at the center of the top layer δ_{i_max} after the CBR test.

$$d'_1 = \frac{H}{n+1} + \delta_{1_max} - a \quad (6)$$

where a is the piston penetration at the end of the CBR tests, which was 20 mm.

After the CBR test, the reinforcement spacing also changed accordingly and was determined as the vertical distance between the center of the reinforcement layer i and that of the reinforcement layer $i+1$ (i.e., the two consecutive layers) in the reinforced specimen. This was calculated as follows:

$$h'_{i,i+1} = \frac{H}{n+1} + \delta_{i+1_max} - \delta_{i_max} \quad (7)$$

The reductions of d_1 and h caused by the piston penetration after the CBR test were also determined through a comparison of these values before and after the test.

$$\Delta h_{i,i+1} = \delta_{i+1_max} - \delta_{i_max} \quad (8)$$

$$\Delta d_1 = d'_1 - d_1 \quad (9)$$

The d_1/B and h/B were used to examine the failure mode of the reinforced specimens (Table 5), with Δd_1 and $\Delta h_{i,i+1}$ indicating the reduction of soil thickness under the piston penetration and between the reinforcement layers after the CBR test, respectively. If the Δd_1 value was small, the soil specimens likely underwent punching shear failure on the topsoil layer caused by the piston penetration. By contrast, a high value Δd_1 indicated compression deformation, with the horizontal movement in the soil layer reflecting the occurrence of shear failure in the soil specimens.

As presented in Table 5, the specimen reinforced with a single reinforcement layer and d_1/B of 1.17 was subject to Failure Mode 1. The high Δd_1 value of the specimens reinforced with a single layer (i.e., approximately 11.6 to 14.7 mm for the three levels of compaction energy listed in Table 6) reflected the significant compression and horizontal movement of soil beneath the piston, which indicated that the shear failure surface occurred above the top reinforcement layer.

Because the ratio of d_1/B and h/B of the specimen reinforced with two reinforcement layers before and after the tests was higher than 0.5, shear failure occurred above the top reinforcement layer

Table 5. Failure modes of reinforced specimens under CBR tests

<i>n</i>	<i>E</i> (kJ/m ³)	<i>h</i> (mm)	At the beginning of test		After 20 mm of piston penetration	
			$d_1/B = h/B$	Failure mode	d'_1/B	$h'_{1,2}/B$
1	486	58.3	1.17	Mode 1	0.89	*
1	1200	58.3	1.17	Mode 1	0.94	*
1	2700	58.3	1.17	Mode 1	0.88	*
2	486	38.8	0.78	Mode 1&2	0.59	0.67
2	1200	38.8	0.78	Mode 1&2	0.60	0.63
2	2700	38.8	0.78	Mode 1&2	0.60	0.61
3	486	29.1	0.59	Mode 1&2	0.46	0.43
3	1200	29.1	0.59	Mode 1&2	0.45	0.44
3	2700	29.1	0.59	Mode 1&2	0.46	0.43
5	486	19.4	0.39	Mode 3	0.37	0.23
5	1200	19.4	0.39	Mode 3	0.37	0.27
5	2700	19.4	0.39	Mode 3	0.38	0.27

(*) Not available

Table 6. Reduction of the distance between piston and the center of the top layer and the reinforcement spacing before and after CBR test

<i>n</i>	<i>E</i> (kJ/m ³)	Δd_1 (mm)	$\Delta h_{1,2}$ (mm)	$\Delta h_{2,3}$ (mm)	$\Delta h_{3,4}$ (mm)	$\Delta h_{4,5}$ (mm)
1	486	13.8	*	*	*	*
1	1200	11.6	*	*	*	*
1	2700	14.7	*	*	*	*
2	486	9.3	7.4	*	*	*
2	1200	9.0	7.7	*	*	*
2	2700	8.8	7.3	*	*	*
3	486	6.1	7.5	3.0	*	*
3	1200	6.7	7.4	3.2	*	*
3	2700	6.2	7.9	3.6	*	*
5	486	1.3	7.8	4.1	1.7	0.7
5	1200	1.0	6.1	4.9	0.7	0.5
5	2700	0.7	6.2	5.4	1.4	0.2

(*) Not available

and between the two reinforcement layers (Failure Mode 1 and 2). As presented in Table 6, both the Δd_1 and $\Delta h_{1,2}$ were greater than 7.3 mm, indicating that the shear failure not only occurred under the piston (Failure Mode 1) but also between the two reinforcement layers (Failure Mode 2). The value of Δd_1 was greater than that of $\Delta h_{1,2}$, especially at the lower compaction energy, which indicated that Failure Mode 1 (more shallow shear failure) dominated in the specimen.

Similarly, for the specimens reinforced with three reinforcement layers, the failure mechanism was a combination of Failure Modes 1 and 2, because the ratios of d_1/B and h/B were both higher than 0.5. As summarized in Table 6, both Δd_1 and $\Delta h_{1,2}$ values were greater than 6.1 mm, indicating that two failure modes occurred in the specimens. Additionally, the $\Delta h_{1,2}$ was higher than Δd_1 , demonstrating that a greater amount of soil movement was induced through shear Failure Mode 2 than through shear Failure Mode 1. The ratio of d'_1/B was less than 0.5, which reduced the shear failure deformation in the soil layer above the top reinforcement layer (Table 5). The influence of piston penetration was reduced significantly in the soil layer between the second and third reinforcement layers, reflected in the $\Delta h_{2,3}$ of approximately 3 to 3.6 mm, which was much lower than the values of Δd_1 and $\Delta h_{1,2}$ (Table 6).

The failure of the specimen reinforced with five reinforcement layers was identified as Failure Mode 3, because both u and h were less than 0.5 at the beginning and end of the test (Table 5). The reduction of the d_1 during the CBR test was small (0.7 to 1.3 mm), representing the occurrence of punching shear failure in the topsoil layer. Conversely, the reductions of reinforcement spacing $\Delta h_{1,2}$ and $\Delta h_{2,3}$ were much higher at over 6.1 and 4.1 mm, respectively (Table 6). Therefore, shear failure occurred in the soil layers between the first and second and the second and third reinforcement layers. The shear failure was not observed at a higher depth, because the reduction of the soil layer thickness between the third and fourth reinforcement layer $\Delta h_{3,4}$ and the fourth and fifth reinforcement layer $\Delta h_{4,5}$ was less than 1.7 and 0.7 mm, respectively. The general shear failure below the last reinforcement layer in Failure Mode 3, as described by [15], was prevented through the restraint capacity of the bottom of the mold.

Finally, the failure mode of the nonwoven geotextile reinforced specimens was not dependent on the compaction energy and the soil density but only on the reinforcement spacing and thickness of the top reinforcement layer (Table 5). This finding is consistent with the results of other studies [11, 12, 15].

4. Conclusions

A series of CBR tests were performed to investigate the bearing capacity of riverbed clay specimens reinforced with nonwoven geotextile layers. The results demonstrated that the reinforcing effects serve to improve the bearing capacity of nonwoven geotextile reinforced clay. Based on the test results, the other conclusions are as follows:

- The nonwoven geotextile significantly increased the CBR value of clay. When the penetration of the piston was less than 6 mm, the specimens reinforced with two nonwoven geotextile layers (i.e., $h/B \approx 0.8$) achieved the highest bearing capacity. When the penetration of the piston exceeded 15 mm, the specimens reinforced with more nonwoven geotextile layers obtained a higher bearing capacity.

- The bearing capacity improvement of the reinforced clay specimens resulted from the soil-reinforcement interaction, membrane tension, and soil density enhancement. Concave deformation of the reinforcement layers was visible in the reinforced specimens after the CBR test, indicating that the membrane tension distributed in enhancing the bearing capacity. The increment of the depth of the reinforcement layer induced a reduction of its maximum deflection. When the geotextile layer is located close to the bottom of the foundation (i.e. its depth is less than $0.4B$), the maximum deflection ratio, R_δ is very high (i.e. up to 0.81). For the reinforcement layers with d_i/B higher than $1.2B$, their maximum deflection ratio was less than 0.3.

- The failure mode of reinforced specimens depends on the thickness of the topsoil layer and reinforcement spacing rather than the soil densities and compaction energy levels. The failure mechanism

of the reinforced specimens was verified through observation of the changes in soil thickness in the reinforced soil specimens.

Finally, the substantial improvement of the bearing capacity of the reinforced clay encourages the usage of nonwoven geotextile reinforced clay as backfill soil for roads or embankments in the rural areas of the Mekong Delta region of Vietnam. The influence of the depth of the reinforcement layers on their concave deformation under loading could be applied to arrange the nonwoven geotextile layers effectively for the flexible pavement designs. In addition, the verified failure modes of reinforced specimens could be used to develop analytical and empirical methods to predict the bearing capacity of geosynthetic reinforced soil. Last, the proposed conclusions are based on the laboratory test results, in which the geosynthetic layer spacing and boundary conditions are different from the field tests. Besides, in the field, the nonuniform and inhomogeneous conditions would be found in the compaction energy, soil properties, and water content.

Acknowledgment

The authors gratefully acknowledge the help and advice of graduate students and lecturers in the Faculty of Civil Engineering, Ho Chi Minh City University of Technology and Education. The comments and suggestions by anonymous reviewers are greatly appreciated.

References

- [1] Transportation Officials (1993). *AASHTO guide for design of pavement structures*. AASHTO.
- [2] Moghaddas-Nejad, F., Small, J. C. (1996). [Effect of geogrid reinforcement in model track tests on pavements](#). *Journal of Transportation Engineering*, 122(6):468–474.
- [3] Kamel, M. A., Chandra, S., Kumar, P. (2004). [Behaviour of subgrade soil reinforced with geogrid](#). *International Journal of Pavement Engineering*, 5(4):201–209.
- [4] Choudhary, A., Gill, K., Jha, J., Shukla, S. (2012). Improvement in CBR of the expansive soil subgrades with a single reinforcement layer. In *Proceedings of Indian Geotechnical Conference*, Indian Geotechnical Society.
- [5] Adams, C. A., Tuffour, Y. A., Kwofie, S. (2016). Effects of soil properties and geogrid placement on CBR enhancement of lateritic soil for road pavement layers. *American Journal of Civil Engineering and Architecture*, 4(2):62–66.
- [6] Keerthi, N., Kori, S. (2018). Study on improvement of sub grade soil using soil-reinforcement technique. *International Journal of Applied Engineering Research*, 13(7):126–134.
- [7] Singh, M., Trivedi, A., Shukla, S. K. (2019). [Strength enhancement of the subgrade soil of unpaved road with geosynthetic reinforcement layers](#). *Transportation Geotechnics*, 19:54–60.
- [8] Koerner, R. M., Narejo, D. (1995). [Bearing capacity of hydrated geosynthetic clay liners](#). *Journal of Geotechnical Engineering*, 121(1):82–85.
- [9] Carlos, D. M., Pinho-Lopes, M., Lopes, M. L. (2016). [Effect of geosynthetic reinforcement inclusion on the strength parameters and bearing ratio of a fine soil](#). *Procedia Engineering*, 143:34–41.
- [10] Rajesh, U., Sajja, S., Chakravarthi, V. K. (2016). [Studies on engineering performance of geogrid reinforced soft subgrade](#). *Transportation Research Procedia*, 17:164–173.
- [11] Binquet, J., Lee, K. L. (1975). [Bearing capacity analysis of reinforced earth slabs](#). *Journal of the Geotechnical Engineering Division*, 101(12):1257–1276.
- [12] Wayne, M. H., Han, J., Akins, K. (1998). The design of geosynthetic reinforced foundations. In *Geosynthetics in Foundation Reinforcement and Erosion Control Systems*, ASCE, 1–18.
- [13] Chen, Q., Abu-Farsakh, M. Y., Sharma, R., Zhang, X. (2007). [Laboratory investigation of behavior of foundations on geosynthetic-reinforced clayey soil](#). *Transportation Research Record: Journal of the Transportation Research Board*, 2004(1):28–38.

- [14] Chen, Q., Abu-Farsakh, M., Sharma, R. (2009). [Experimental and analytical studies of reinforced crushed limestone](#). *Geotextiles and Geomembranes*, 27(5):357–367.
- [15] Chen, Q., Abu-Farsakh, M. (2015). [Ultimate bearing capacity analysis of strip footings on reinforced soil foundation](#). *Soils and Foundations*, 55(1):74–85.
- [16] ASTM D 1557-12 (2015). *Compaction characteristics of soil using modified effort (56,000 ft-lbf/ft³(2,700 kN-m/m³))*. West Conshohocken, PA, USA.
- [17] Nguyen, M. D., Yang, K. H., Lee, S. H., Wu, C. S., Tsai, M. H. (2013). [Behavior of nonwoven-geotextile-reinforced sand and mobilization of reinforcement strain under triaxial compression](#). *Geosynthetics International*, 20(3):207–225.
- [18] ASTM D 1883-14 (2016). *Standard test method for California bearing ratio (CBR) of laboratory-compacted soils*. ASTM International, West Conshohocken, PA, USA.
- [19] Berg, R. R., Christopher, B. R., Samtani, N. C. *Design and construction of mechanically stabilized earth walls and reinforced soil slopes*. Vol. FHWA-NHI-10-024, US Department of Transportation, Federal Highway Administration.
- [20] Perkins, S. W., Ismeik, M. (1997). [A synthesis and evaluation of geosynthetic-reinforced base layers in flexible pavements - Part I](#). *Geosynthetics International*, 4(6):549–604.
- [21] Chakraborty, M., Kumar, J. (2014). [Bearing capacity of circular foundations reinforced with geogrid sheets](#). *Soils and Foundations*, 54(4):820–832.
- [22] Abu-Farsakh, M., Chen, Q., Sharma, R. (2013). [An experimental evaluation of the behavior of footings on geosynthetic-reinforced sand](#). *Soils and Foundations*, 53(2):335–348.
- [23] Abduljawwad, S. N., Bayomy, F., Al-Shaikh, A.-K. M., Al-Amoudi, O. S. B. (1994). [Influence of geotextiles on performance of saline sebkha soils](#). *Journal of Geotechnical Engineering*, 120(11):1939–1960.
- [24] Adams, C. A., Tuffour, Y. A., Kwofie, S. (2016). Effects of soil properties and geogrid placement on CBR enhancement of lateritic soil for road pavement layers. *American Journal of Civil Engineering and Architecture*, 4(2):62–66.
- [25] Giroud, J.-P., Noiray, L. (1981). [Geotextile-Reinforced Unpaved Road Design](#). *Journal of the Geotechnical Engineering Division*, 107(9):1233–1254.
- [26] Yang, K.-H., Yalaw, W. M., Nguyen, M. D. (2016). [Behavior of geotextile-reinforced clay with a coarse material sandwich technique under unconsolidated-undrained triaxial compression](#). *International Journal of Geomechanics*, 16(3).
- [27] Wang, J.-Q., Zhang, L.-L., Xue, J.-F., Tang, Y. (2018). [Load-settlement response of shallow square footings on geogrid-reinforced sand under cyclic loading](#). *Geotextiles and Geomembranes*, 46(5):586–596.
- [28] Kumar, A., Saran, S. (2003). [Bearing capacity of rectangular footing on reinforced soil](#). *Geotechnical and Geological Engineering*, 21(3):201–224.